Rare Metal Materials and Engineering
Volume 49, Issue 6, June 2020
Available online at www.rmme.ac.cn

Science Press

Cite this article as: Rare Metal Materials and Engineering, 2020, 49(6): 1825-1833.

ARTICLE

Hot Tensile Behavior and Microstructure Evolution Mechanism of Ti_2AlNb Sheet

Wu Yong[1,2], Wang Dongjun[2,3], Fan Ronglei[1], Liu Zhiqiang[2,3], Liu Gang[2,3]

[1] Nanjing University of Aeronautics and Astronautics, Nanjing 210016, China; [2] National Key Laboratory for Precision Hot Processing of Metals, Harbin Institute of Technology, Harbin 150001, China; [3] Institute of High Pressure Fluid Forming, Harbin Institute of Technology, Harbin 150001, China

Abstract: The hot tensile behavior of Ti-22Al-24.5Nb-0.5Mo (at%) alloy was investigated by the hot tensile tests in the temperature range of 910~1040 °C and strain rate range of 0.0001~0.1 s^{-1}. The Arrhenius equations were calculated at the three different phase fields and the microstructure evolution mechanisms were studied by microstructure observation. The results show that the activation energies are 759.43, 516.71 and 438.59 kJ/mol at B2/β+O, α_2+B2/β+O and α_2+B2/β phase fields, respectively. The microstructure evolution is dominated by dynamic recrystallization of O-phase and dynamic recovery of B2/β phase grains, and the softening mechanism is the globularization of O lamellar grains at B2/β+O phase field, while the softening mechanism is dynamic recrystallization and shear bands of the B2/β-phase grains at α_2+ B2/β+O phase field.

Key words: Ti_2AlNb alloy; hot tensile test; microstructure evolution; Arrhenius equation

Ti_2AlNb alloy has many excellent properties, such as high specific strength, good creep resistance, oxidation resistance[1-4]. It was considered as a potential lightweight structural material at high-temperatures from 600 °C to 800 °C in aerospace industry. As a typical composition of the third generation of Ti_2AlNb alloys, Ti-22Al-(23~27)Nb exhibits good ductility and creep resistance[5,6] and shows a wide application prospect as the complex shell parts in the aerospace field[7,8]. However, because of the brittleness and poor formability, Ti_2AlNb alloy has a narrow temperature and strain rate window for hot workability. Hot forming is a good choice for deforming complex shell parts and has been widely applied for some materials[9,10]. Meanwhile, for the purpose of optimizing the hot forming parameters of Ti_2AlNb alloy, it is necessary to investigate the hot deformation behavior and microstructure evolution. The stress-strain curves and processing maps of the homogenized ingot[11], arc skull melted[12] and powder metallurgy[13] of Ti-22Al-25Nb alloy have been measured by isothermal compression tests. However, there is seldom research on the hot tensile behavior and microstructure evolution of the Ti_2AlNb rolled sheet. In view of the three phase fields from 910 °C to 1040 °C for Ti_2AlNb alloy [1,14], the microstructure evolution and phase transformation are various at different deformation temperatures[4]. Meanwhile, the phase components and microstructure of Ti_2AlNb-alloy strongly affect its mechanical properties[15]. Therefore, it is also necessary to study the microstructure evolution of the alloy during the hot tensile tests.

In this study, the hot tensile behavior of Ti_2AlNb alloy was studied at different constant strain rates at elevated temperatures. The stress-strain curves at constant tensile strain rates were obtained. The Arrhenius equations were calculated to optimize the forming process at B2/β+O, α_2+B2/β+O and α_2+B2 phase fields. The microstructure evolution was investigated by backscattered electron (BSE) image and electron back scattering diffraction (EBSD). Furthermore, the mechanism of deformation with different process parameters was discussed. The work aims to further understand the hot deformation mechanism and to promote the hot forming process of Ti_2AlNb rolled sheet.

Received date: June 15, 2019
Foundation item: National Natural Science Foundation of China (51805256); High-level Personnel of Special Support Program (W02020239)
Corresponding author: Liu Gang, Ph. D., Professor, National Key Laboratory for Precision Hot Processing of Metals, Harbin Institute of Technology, Harbin 150001, P. R. China, E-mail: Gliu@hit.edu.cn

1 Materials and Experimental Procedure

The nominal chemical composition of the sheet is Ti-22Al-24.5Nb-0.5Mo. The as-received sheet was forged and rolled at α_2+B2/β+O phase field. After the last rolling, the sheet was heat treated at α_2+B2/β+O phase field for 2 h and aged at 800 °C for 10 h. The thickness of the as-received sheet was 2.0 mm. The uniaxial tensile tests were carried out on the instron-5500R testing machine. The gauge size of the "dog bone" tensile sample was 4 mm×15 mm and the tensile direction was parallel to the rolling direction of the sheet. In order to obtain the tensile result at a constant true strain rate, the machine was equipped with a feedback control system to impose exponential increase of the actuator speed. The tensile speed was calculated as follows[16]:

$$v = \dot{\varepsilon} L_0 \exp(\dot{\varepsilon} t) \quad (1)$$

where v is the cross head velocity, $\dot{\varepsilon}$ is the strain rate, L_0 is the gauge length of the specimen, and t is the tensile time. Before the tensile test, the samples were put into the heating furnace for 15 min to adjust the material and furnace's temperature distribution. After tensile tests, the specimen was taken out quickly and water quenched to reserve the high temperature microstructure. The microstructure of the deformed specimens was observed by BSE and EBSD. The BSE and EBSD test were conducted by a ZEISS Supra 55 SAPPHIRE and the EBSD data was analyzed by the software CHANNAL.5.

2 Results and Discussion

2.1 Initial microstructure

Fig.1 shows the BSE image of as-received sheet. Since the relatively brighter zone in the BSE image exhibits relatively higher average atomic number, the bright, gray and dark zones represent the B2/β, O and α_2 phases, respectively. The fine B2/β and lamella O grains are the matrix structure, and the equiaxed α_2 grains are uniformly distributed in the materials. The thicknesses of the fine lamella O grains are smaller than 0.1 μm.

Fig.2 shows the EBSD results of the as-received sheet. Fig.2a shows the phase map. The volume fractions of α_2, B2/β and O phase are 10.6 vol%, 21.7 vol% and 67.7 vol%, respectively. Fig.2b shows the local misorientation (LM) map, where the black thick lines represent the high-angle grain boundary (HAGBs, >10°) and the blue fine lines represent the low-angle grain boundary (LAGBs, 2~10°). The LM value shows the distribution of the residual stress, where the high LM value represent the high residual stress. It can be found that the LM value of B2/β phase is higher than that of α_2 and O phase, which shows that residual stress in B2/β phase is higher than that in α_2 and O phase.

2.2 Hot tensile behavior

Fig.3a shows the tensile speed comparison between the constant tensile speed and constant strain rate tests. Fig.3b shows the tensile results at 950 and 985 °C with strain rate of

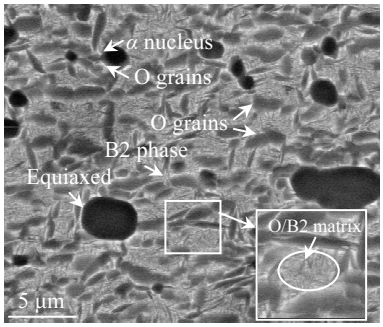

Fig.1 BSE image of Ti_2AlNb rolled sheet

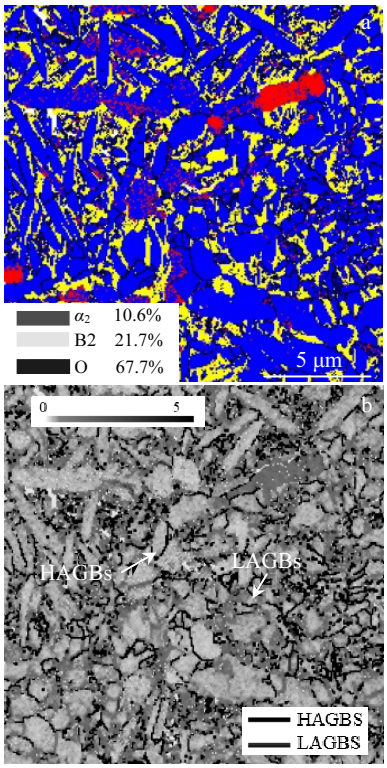

Fig.2 EBSD results of as-received Ti_2AlNb sheet: (a) phase map and (b) local misorientation map

0.001 s^{-1}. Obviously, there is a big difference between the two test methods. The strain softening phenomenon of the constant tensile speed tensile method is higher than that of the constant strain rate tensile method. In order to establish the constitutive equations and processing map based on the true stress-strain curves at a certain strain rate, the new tensile method with constant strain rate was adopted in this work.

Fig.4 shows the true stress-strain curves of Ti_2AlNb at elevated temperatures. It can be seen that the flow stress is significantly affected by the deformation temperature, strain and strain rate. The flow curve can be divided into three stages in the tensile test[17]. At the early stage, the flow stress increa-

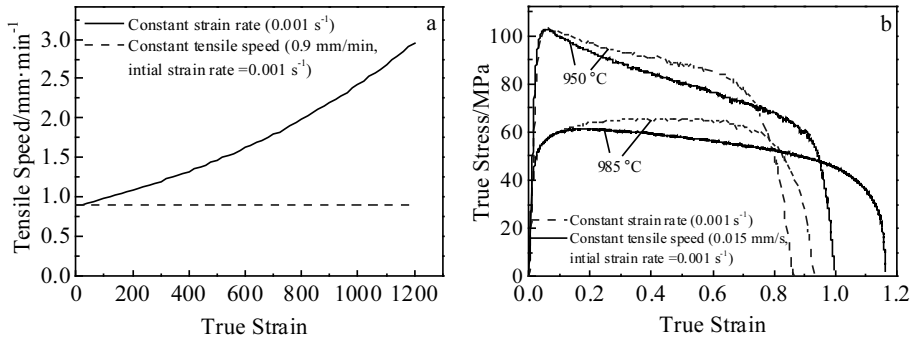

Fig.3 Comparison of two different tensile results: (a) tensile speeds and (b) true stress-strain curves

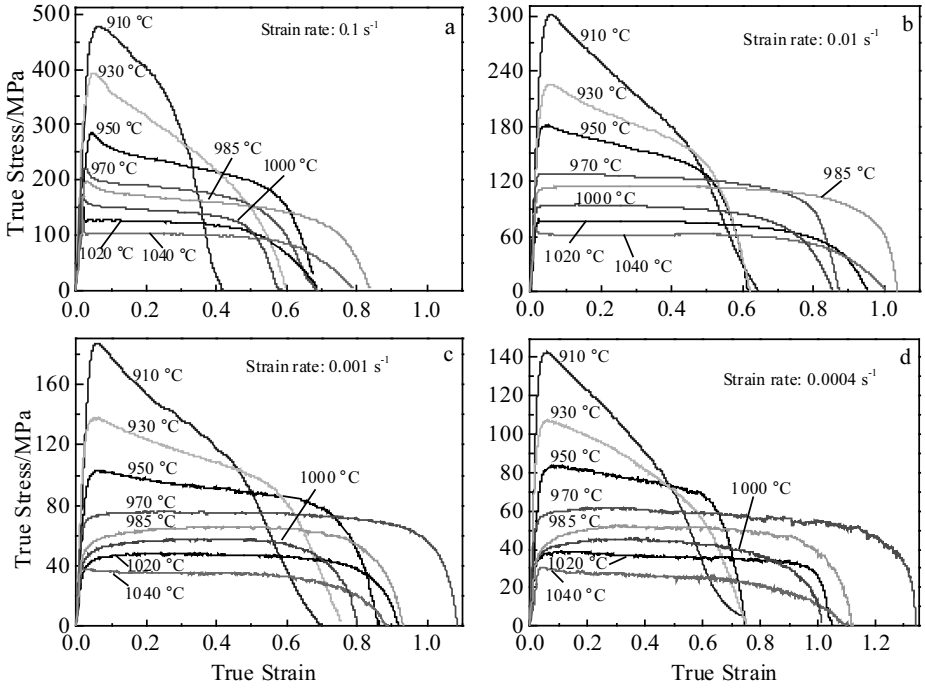

Fig.4 Ture stress-strain curves at different strain rates: (a) 0.1 s^{-1}, (b) 0.01 s^{-1}, (c) 0.001 s^{-1}, and (d) 0.0004 s^{-1}

ses to the peak sharply. At the second stage, the steady plastic deformation occurs during the tensile test. At the third stage, the slope of the curves initially changes and the localized necking occurs in the specimens until fracture. Obviously, with increasing the true strain, the changes of the flow stresses are various at different tensile temperatures. The flow stress linearly drops with temperature from 910~950 °C. Within the temperature of 970~1040 °C, the flow stress is steady. The change of the flow stress results in various deformation behaviors in different phase fields[18, 19]. There are four phase fields from 900 °C to 1100 °C, i.e. B2/β+O (<970 °C), α_2+B2/β+O (970~1010 °C), α_2+B2/β (1010~1060 °C) and B2/β (>1060 °C).

Fig.5 shows the relationship among peak stress, temperature and strain rate. At a certain strain rate, the peak stress decreases with increasing the temperature. At the same temperature, the peak stress decreases with reducing the strain rate. It can be found that there is an inflection point at 970 °C and the reducing rate of peak stress in temperature range of 910~970 °C is larger than that in temperature range of 970~1040 °C.

Fig.6a shows the total elongation of the specimens. The bigger the elongation, the better the formability. For the strain rate of 0.001 and 0.0004 s^{-1}, the formability of Ti_2AlNb sheet fluctuates with increasing the forming temperature. The as-received sheet presents excellent formability at 970 °C, at which the elongation is 196.4% and 281.3% at the strain rates of 0.001 and 0.0004 s^{-1}, respectively. For the strain rate of 0.1 and 0.01 s^{-1}, the effect of temperature on the formability is nearly the same to that at the strain rate of 0.001 and 0.0004 s^{-1}, except that it presents the best formability at 985 °C.

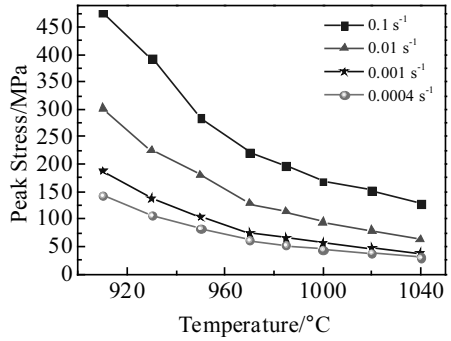

Fig.5 Relationship among peak stress, temperature and strain rate

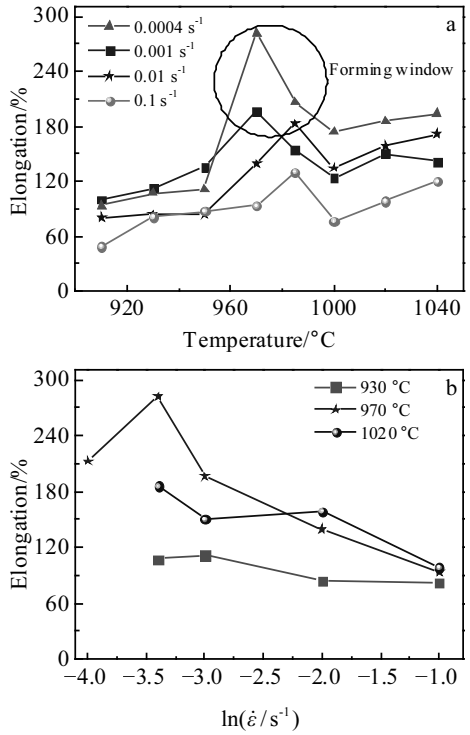

Fig.6 Elongation of specimens at different forming temperatures (a) and strain rates (b)

Meanwhile, the formability is affected by the strain rate, as shown in Fig.6b. For a certain forming temperature, there is an optimal range of strain rates. When the strain rate is larger or less than the optimal strain rate, the formability is worse. According to the elongation results of Ti_2AlNb, the rolled sheet has an optimum forming window at temperature of 970~985 °C and strain rate of 0.001~0.0004 s^{-1}.

2.3 Arrhenius constitutive equation

During the hot deformation, the flow stresses are affected by the strain rate, forming temperature and deformation degree. The Arrhenius equation is a typical equation to describe the flow stress:

$$\dot{\varepsilon} = A'[\sinh(\alpha'\sigma)]^{n^*} \exp(-Q/RT) \quad (2)$$

where $\dot{\varepsilon}$ is the strain rate (s^{-1}), σ is the flow stress (MPa), Q is the hot deformation activation energy, n^* is the stress exponent ($n^*=1/m$), m is the strain rate sensitivity exponent, T is the temperature (K), R is the gas constant (8.314 $J\cdot mol^{-1}\cdot K^{-1}$), and A' and α' are the material constants.

It can also be given by the Zener-Hollomon parameters as follows[13]:

$$\ln Z = \ln\dot{\varepsilon} + \frac{Q}{RT} = \ln A' + n^* \ln[\sinh(\alpha'\sigma)] \quad (3)$$

where Z is the Zener-Hollomon parameter. $\alpha' = \beta'/n_1$, $n_1 = \partial\ln\dot{\varepsilon}/\partial\ln\sigma$ and $\beta' = \partial\ln\dot{\varepsilon}/\sigma$. β' is the material constant. The Arrhenius equations are solved at B2/β+O phase field (910, 930, 950 and 970 °C), α_2+B2/β+O phase field (970, 985 and 1000 °C) and α_2+B2/β phase field (1000, 1020 and 1040 °C). The material parameters of n_1 and β' are solved in Fig.7a and Fig.7b. Then the α' values are calculated as 0.0056, 0.0093 and 0.0124 at B2/β+O, α_2+B2/β+O and α_2+B2/β phase field, respectively. Fig.7c and Fig.7d show the relationship of $\ln[\sinh(\alpha'\sigma)]$-$\ln\dot{\varepsilon}$ and $\ln[\sinh(\alpha'\sigma)]$-$T^{-1}$, respectively. Then, the values of n^* and ν' can be calculated by $n^* = \left[\frac{\partial\ln\dot{\varepsilon}}{\partial\ln[\sinh(\alpha'\sigma)]}\right]_T$ and $\nu' = \frac{\partial\ln[\sinh(\alpha'\sigma)]}{\partial\ln(1/T)}$.

At B2/β+O phase field, n^* and ν' are 3.19 and 28.64. At α_2+B2/β+O phase field, n^* and ν' are 3.02 and 20.56. At α_2+B2/β phase field, n^* and ν' are 3.10 and 17.01. According the calculating equation of hot deformation activation energy, i.e., $Q=R\nu n^*$, the Q is calculated as 759.43, 516.71 and 438.59 kJ/mol for B2/β+O, α_2+B2/β+O, α_2+B2/β phase field, respectively. Based on the above results, the flow stress of Ti_2AlNb sheet can be described as follows:

$$\begin{cases} \sigma = \dfrac{1}{0.0056}\ln\left\{\left(Z/e^{69.47}\right)^{1/3.11} + \left[\left(Z/e^{69.47}\right)^{2/3.11} + 1\right]^{1/2}\right\} \\ Z = \dot{\varepsilon}\exp\left(759.43/RT\right) \end{cases}$$

(B2/β+O field phase) (4)

$$\begin{cases} \sigma = \dfrac{1}{0.0093}\ln\left\{\left(Z/e^{43.83}\right)^{1/3.09} + \left[\left(Z/e^{43.83}\right)^{2/3.09} + 1\right]^{1/2}\right\} \\ Z = \dot{\varepsilon}\exp\left(516.71/RT\right) \end{cases}$$

(α_2+B2/β+O field phase) (5)

$$\begin{cases} \sigma = \dfrac{1}{0.0124}\ln\left\{\left(Z/e^{35.27}\right)^{1/2.96} + \left[\left(Z/e^{35.27}\right)^{2/2.96} + 1\right]^{1/2}\right\} \\ Z = \dot{\varepsilon}\exp\left(438.60/RT\right) \end{cases}$$

(α_2+B2/β field phase) (6)

2.4 Microstructure evolution of Ti_2AlNb alloy

2.4.1 Effect of temperature on microstructure evolution

Fig.8 shows the BSE images of the un-deformation and deformation zone for the tensile specimens with strain rate of 0.001 s^{-1}. It can be found that the O-phase volume fraction is

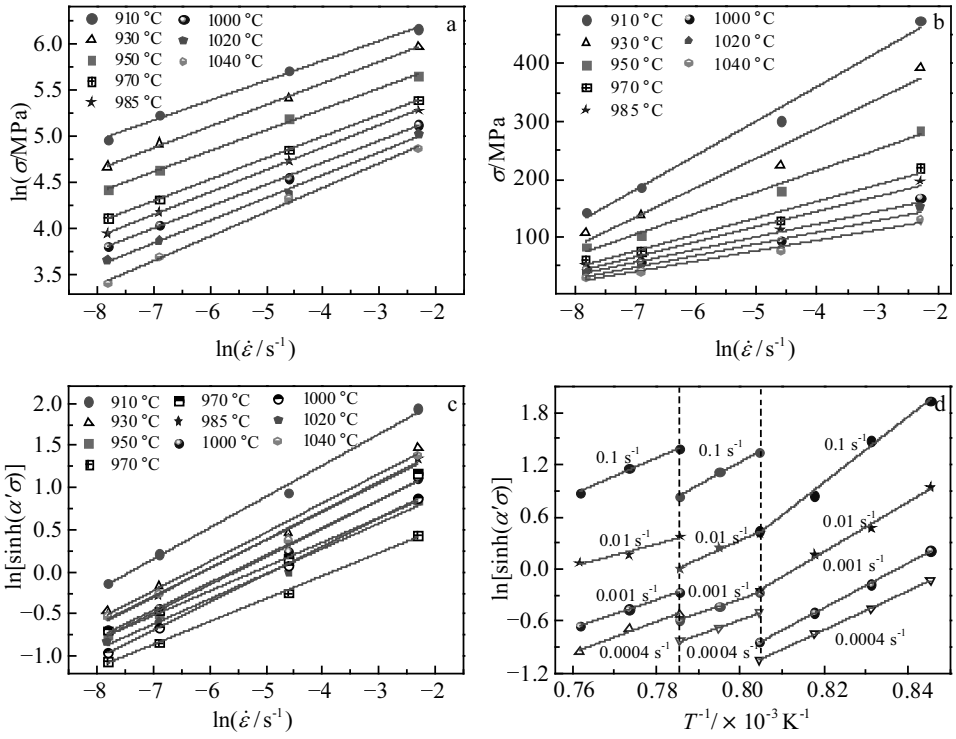

Fig.7 Solving of Arrhenius equation: (a) $\ln\sigma$-$\ln\dot{\varepsilon}$, (b) σ-$\ln\dot{\varepsilon}$, (c) $\ln[\sinh(\alpha'\sigma)]$-$\ln\dot{\varepsilon}$, and (d) $\ln[\sinh(\alpha'\sigma)]$-$T^{-1}$

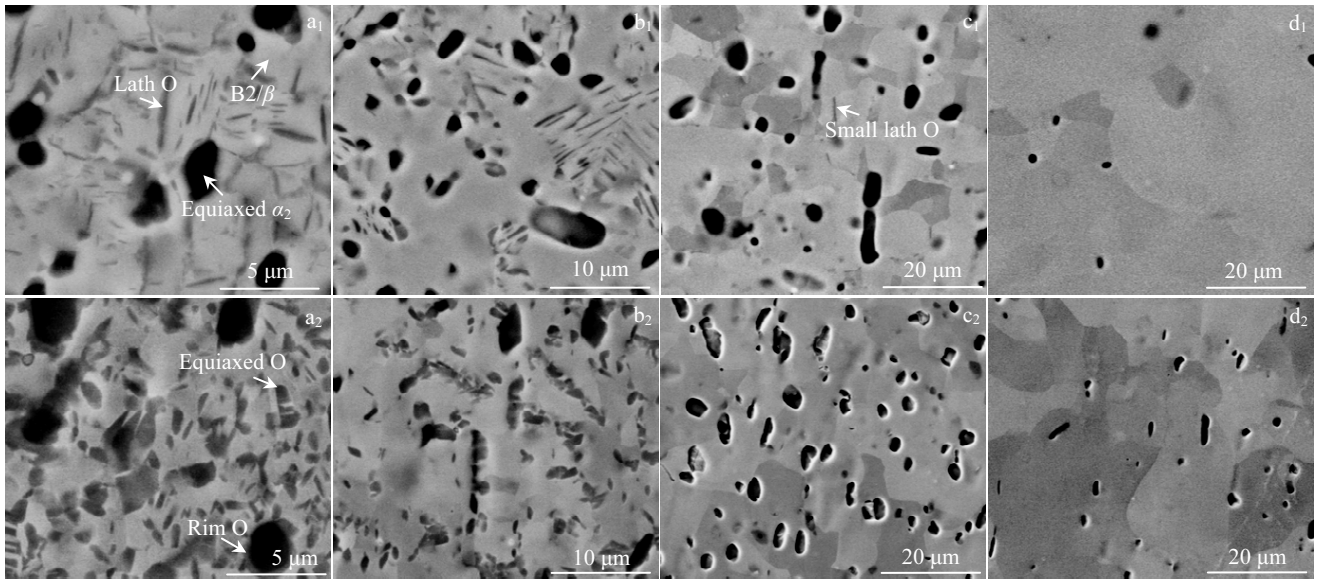

Fig.8 BSE images of un-deformation (a_1~d_1) and deformation (a_2~d_2) zone for the tensile tested specimens at strain rate of 0.001 s^{-1}: (a_1, a_2) 930 °C, (b_1, b_2) 950 °C, (c_1, c_2) 970 °C, and (d_1, d_2) 1020 °C

reduced with increasing the forming temperature. In Fig.8a_1 and Fig.8a_2, it can be found that the O-phase volume fraction remains stable during the hot deformation. However, the lamella O-phase grains are broken and changed to the equiaxed grains. Meanwhile, some rim O-phase grains appear around the equiaxed α_2 grains, the same in Fig.8b_1 and Fig.8b_2. The microstructure evolution results at 930 and 950 °C show that the O-phase grain shape is affected by the plastic deformation. At 970 and 1020 °C, the volume fraction of O-phase is very low. The effect of O-phase grain on hot

deformation can be ignored. Therefore, the flow stress is mainly affected by the B2/β and α_2 phase grains. Fig.8c_1, 8c_2, 8d_1, 8d_2 show that the α_2-phase equiaxed grains remain steady during the hot deformation, which indicates that the α_2-phase grains are hard grains at high temperatures.

Fig.9 shows the EBSD results of the deformation zone for the tensile tested specimens. Fig.9a_1~9d_1 show the phase maps. Fig.9a_2~9d_2 show the LM value maps. The B2/β grain boundaries can be observed by the BESD tests. In Fig.9a_1 and Fig.9b_1, the volume fractions of O-phase are 32.4 vol% and 16.9 vol% at 930 and 950 °C, respectively. Plenty of small recrystallized grains are huddled together in the same orientation, just like a necklace. Meanwhile, some O-phase and α_2-phase grains are mixed together. It can be found that dynamic recrystallization occurs in the O-phase grains at 930 and 950 °C. In Fig.9a_2 and Fig.9b_2, the LM value of O-phase and α_2-phase is larger than that of B2/β-phase, which is the opposite result for the as-received sheet in Fig.2b. It means that the rolled dislocations in B2/β-phase grains of the as-received samples are repaired by the heating and hot deformation. While, plenty of deformation dislocations are also generated in O-phase and α_2-phase grains.

Fig.9c_1 and Fig.9d_1 show the phase maps at 970 and 1020 °C, and Fig.9c_2 and Fig.9d_2 show the LM maps. The true strains of the specimens are 0.6. With increasing the forming temperature, the volume fraction of O-phase and α_2-phase significantly decreases and the grain size of B2/β increases. The results are the same as the BSE test results. The mean grain sizes of the B2/β phase are 3.7, 12.1 and 20.1 μm at 930, 970 and 1020 °C, respectively. There are also some recrystallized B2/β grains at big B2/β grain boundaries[13].

2.4.2 Effect of strain rate on microstructure evolution

Fig.10 shows the LM images and the strain contours of the tensile tested specimens at 985 °C with different strain rates. The strain contours show the strain concentration map, which is calculated by the grain orientation relationship. The phase maps are not analyzed because the volume fractions of α_2, B_2/β and O phase are nearly the same at the same temperature. However, the LM images and strain contours are significantly different. Fig.10a, 10c, 10e and 10g show the LM maps of the tested specimens with strain rate of 0.1, 0.01, 0.001, and 0.0004 s^{-1}.

In addition, Fig.11 shows the effects of strain rates on LM value distribution and B2/β phase average sub-grain size. With the increase of the strain rate, the average sub-grain size of B2/β phase significantly decreases, and the LM value and the residual stress of the material increase. When the strain rate is high (0.01~0.1 s^{-1}), an obvious localized deformation shear band appears, and the angle between the shear band and the tensile direction is 20°~30°. At the shear band zone, there are a plenty of small recrystallized B2/β grains. When the strain rate decreases to 0.001 and 0.0004 s^{-1}, the deformation is homogenized and there are no obvious deformation shear bands. Actually, the LM value represents the materials dislocation density and residual stress.

Fig.12 shows the TEM images of the tensile tested specimens at 985 °C with strain rate of 0.1 and 0.001 s^{-1}. It can be found that there are plenty of dislocation walls in the tensile

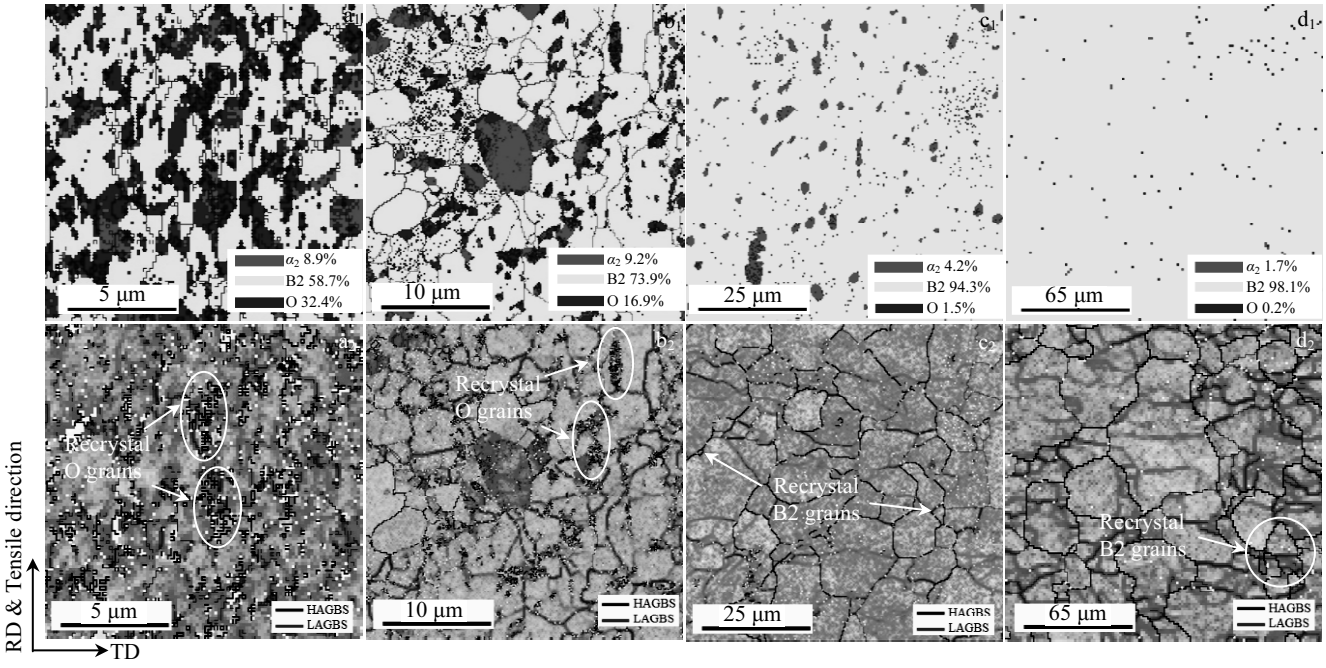

Fig.9 Phase maps (a_1~d_1) and LM maps (a_2~d_2) for the tested specimens at strain rate of 0.001 s^{-1}: (a_1, a_2) 930 °C, (b_1, b_2) 950 °C, (c_1, c_2) 970 °C, and (d_1, d_2) 1020 °C

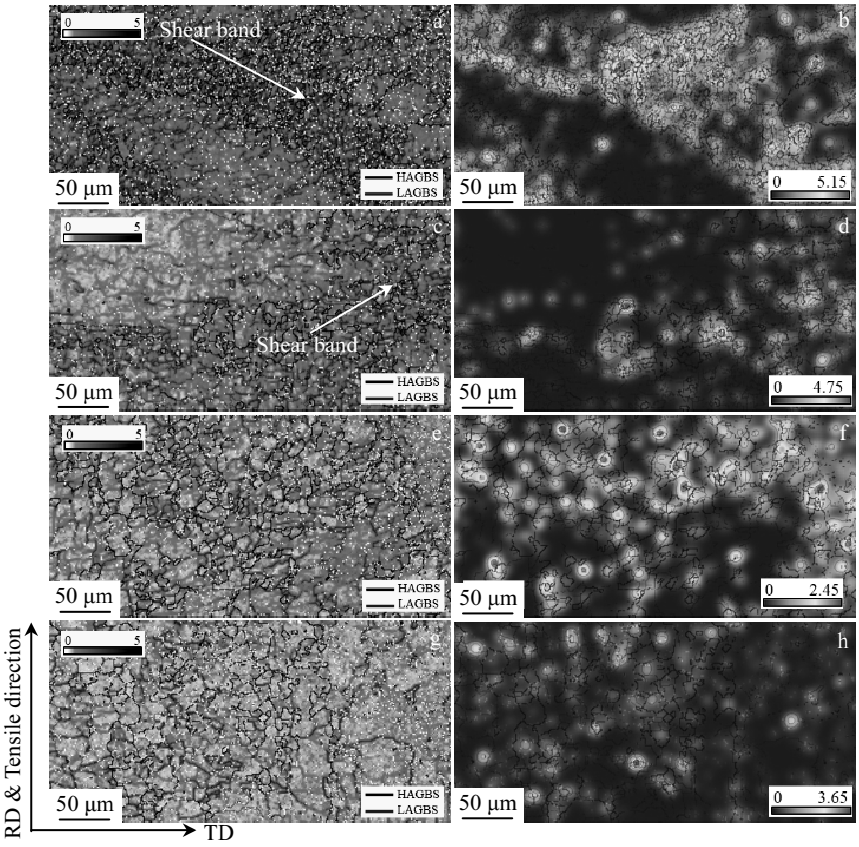

Fig.10 LM images (a, c, e, g) and strain contours (b, d, f, h) of the tested specimens at 985 °C with true strain of 0.6: (a, b) 0.1 s^{-1}, (c, d) 0.01 s^{-1}, (e, f) 0.01 s^{-1}, and (g, h) 0.0004 s^{-1}

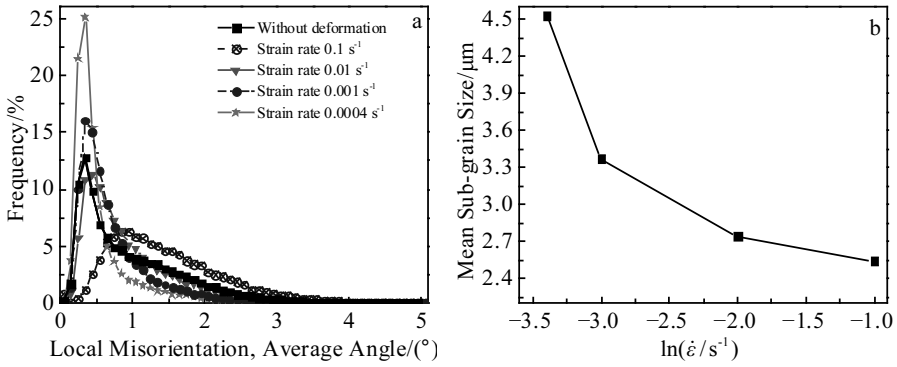

Fig.11 Effect of strain rate on LM value (a) and sub-grain size (b) at 985 °C during tensile tests

specimen with stain rate of 0.1 s^{-1}. Obviously, the flow stress and the microstructure of the tensile specimens are affected by the strain rate. In Fig.4, the strain softening occurs in the tensile specimens with high strain rates (0.01~0.1 s^{-1}), while there is no strain softening in the tensile specimens with low strain rates (0.0004~0.001 s^{-1}). The strain softening phenomenon is due to the change of mean grain size and the material damage of the shear bands. Fig.10b, 10d, 10f, 10h show the strain contours of the tested specimens with strain rate of 0.1, 0.01, 0.001 and 0.0004 s^{-1}, respectively. Obviously, the strain of the shear band zone is larger than that of the normal zone.

2.4.3 Microstructure evolution characteristics

As mentioned above, it is important to note that the deformation activation energies are different in the three phase fields because of the difference in the microstructure evolution

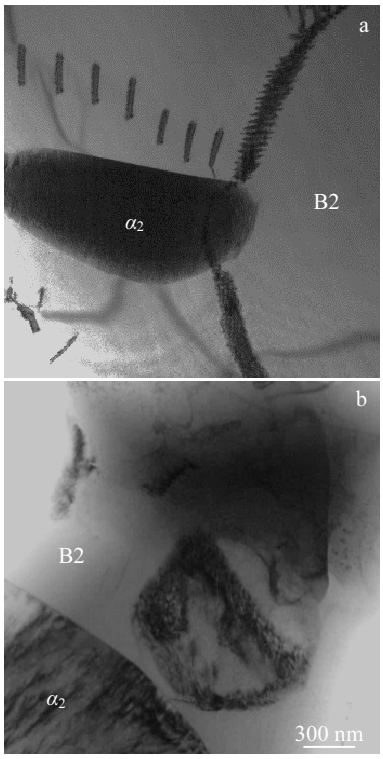

Fig.12 TEM images of the tensile tested specimens at 985 °C with strain rate of 0.1 s^{-1} (a) and 0.001 s^{-1} (b)

characteristics. The metal hot deformation mechanisms, i.e., the dislocation motion, grain boundary sliding and diffusion creep, are controlled by the metal thermal activation energy. During the hot deformation process, the flow stresses are affected by the comprehensive results of the three deformation mechanisms. Meanwhile, the flow stress is also affected by the grain shape, grain size, phase volume fraction, materials damage, etc.

For B2/β+O phase field, the O-phase volume fraction is about 10 vol~50 vol%, while the α_2-phase volume fraction is about 10 vol%. The average value of activation energy Q is 759.43 kJ/mol. The high activation energy and softening are mainly related to the globularization of O lamellar structure[12]. Meanwhile, the flow stress linearly drops during the tensile tests, presenting liner softening phenomenon. In Fig.8 and Fig.9, there are few HAGBs in B2/β grains, while many small recrystallized O-phase grains are generated during the deformation, indicating that the O-phase grains are participated in the plastic deformation. Therefore, the main microstructure evolution characteristics are the dynamic recrystallization of O-phase and dynamic recovery of B2/β grains in B2/β+O phase field. The main softening mechanism is the globularization of O lamellar structure.

At α_2+B2/β+O phase field, most α_2/O grains are evolved into B2/β grains, as shown in Fig.9. The average value of activation energy Q is 516.71 kJ/mol. At high strain rates (such as 0.1 s^{-1}), once the plastic deformation begins, the flow stress immediately drops linearly, which shows the significant softening phenomenon in Fig.4a. The EBSD results in Fig.10 show that plenty of small recrystallized B2/β grains exist at the shear band zone. So the main softening mechanism is dynamic recrystallization of the B2/β-phase grains. When the strain rate is 0.001~0.0004 s^{-1}, the flow stress remains steady. There is a dynamic equilibrium between grain growth and recrystallization grain refinement of B2/β-phase grains.

At α_2+B2/β phase field, most α_2/O grains are evolved into B2/β grains. The B2/β grains are coarser than those in the deformation of α_2+B2/β+O phase field because of the decrease of the pinning effect of tiny α_2 and O grains. The microstructure evolution has been studied by many researches[13]. The main microstructure evolution mechanism is the dynamic recrystallization of B2/β grains.

3 Conclusions

1) The formability of Ti_2AlNb rolled sheet is affected by the forming temperature and strain rate. The appropriate hot deformation parameters are temperatures of 970~985 °C and strain rate of 0.001~0.0004 s^{-1}. The Ti-22Al-24.5Nb-0.5Mo alloy exhibits the optimal plasticity, with a large elongation of 281.3% at 970 °C with strain rate of 0.0004 s^{-1}.

2) The Arrhenius equations are calculated at 910~1040 °C. The activation energies are 759.43, 516.71 and 438.59 kJ/mol at B2/β+O, α_2+B2/β+O and α_2+B2/β phase fields, respectively.

3) The microstructure evolution characteristics are various at different forming temperatures and strain rates during the hot deformation. For deformation in B2/β+O phase field, the microstructure changes are dominated by dynamic recrystallization of O-phase and dynamic recovery of B2/β phase grains. The softening mechanism is the globularization of α_2/O lamellar grains. For deformation in α_2+B2/β+O phase field at strain rate of 0.01~0.1 s^{-1}, the main softening mechanism is dynamic recrystallization and shear bands of the B2/β phase grains. When the strain rate is reduced to 0.0004~0.001 s^{-1}, there is a dynamic equilibrium between grain growth and recrystallization grain refinement of B2/β phase grains. For deformation in α_2+B2/β phase field at strain rate of 0.001 s^{-1}, the microstructure evolution is dominated by the dynamic recrystallization of B2/β phase grains.

References

1 Banerjee D. *Philosophical Magazine Part A*[J], 1995, 72(6): 1559
2 Boehlert C J, Miracle D B. *Metallurgical & Materials Transactions A*[J], 1999, 30(9): 2349
3 Boehlert C J. *Metallurgical & Materials Transactions A*[J], 2001, 32(8): 1977
4 Jiao X Y, Liu G, Wang D J *et al*. *Materials Science & Engineering A*[J], 2017, 680: 182
5 Gogia A K, Nandy T K, Banerjee D *et al*. *Intermetallics*[J], 1998,

6(7-8): 741
6 Dey S R, Suwas S, Fundenberger J J *et al*. *Intermetallics*[J], 2009, 17(8): 622
7 Kong B, Liu G, Wang D *et al*. *Materials & Design*[J], 2016, 90: 723
8 Du Z, Jiang S, Zhang K *et al*. *Materials & Design*[J], 2016, 104: 242
9 Wu Y, Liu G, Liu Z *et al*. *Materials & Design*[J], 2016, 108: 298
10 Zhang X Y, Li M Q, Li H *et al*. *Materials & Design*[J], 2010, 31(6): 2851
11 Boehlert C J. *Materials Science & Engineering A*[J], 2000, 279(1): 118
12 Ma X, Zeng W, Xu B *et al*. *Intermetallics*[J], 2012, 20(1): 1
13 Jia J, Zhang K, Jiang S. *Materials Science & Engineering A*[J], 2014, 616: 93
14 Zhang H, Li H, Guo Q *et al. Journal of Materials Research*[J], 2016, 31(12): 1764
15 Xue C, Zeng W, Wang W *et al*. *Materials Science & Engineering A*[J], 2013, 587: 54
16 Kotkunde N, Krishnamurthy H N, Puranik P *et al. Materials and Design*[J], 2014, 54(2): 96
17 Lin P, He Z, Yuan S *et al. Materials Science & Engineering A*[J], 2012, 556(11): 617
18 Wang W, Zeng W, Liu Y *et al. Journal of Materials Engineering & Performance*[J], 2018, 27(1): 293
19 Dang W, Li J, Zhang T *et al*. *Journal of Materials Engineering & Performance*[J], 2015, 24(10): 3951

Ti_2AlNb 板材的热拉伸行为和微观组织演化机理

武　永[1,2]，王东君[2,3]，范荣磊[1]，刘志强[2,3]，刘　钢[2,3]

(1. 南京航空航天大学，江苏 南京 210016)

(2. 哈尔滨工业大学 金属精密热加工国家级重点实验室，黑龙江 哈尔滨 150001)

(3. 哈尔滨工业大学 流体高压成形技术研究所，黑龙江 哈尔滨 150001)

摘　要：通过高温拉伸试验研究了 Ti-22Al-24.5Nb-0.5Mo 合金在温度范围为 910~1040 ℃、应变速率为 0.0001~0.1 s^{-1} 条件下的高温变形行为。建立了 B2/β+O、α_2+B2/β+O 和 α_2+B2/β 3 个不同相区的 Arrhenius 方程，并通过多种微观组织观察技术研究了微观组织演化机理。结果表明：在 B2/β+O、α_2+B2/β+O 和 α_2+B2/β 3 个相区的激活能分别为 759.43，516.7 和 438.59 kJ/mol。微观组织演化主要是 O 相晶粒的动态再结晶和 B2/β 相晶粒的动态回复，在 B2/β+O 相区的软化机制是片层 O 相晶粒的球化，而在 α_2+B2/β+O 相区的软化机制是 B2/β 相晶粒的动态再结晶及局部剪切带的形成。

关键词：Ti_2AlNb 合金；高温拉伸；组织演变；Arrhenius 方程

作者简介：武　永，男，1986 年生，博士生，南京航空航天大学机电学院，江苏 南京 210016，E-mail: wuyong@nuaa.edu.cn